

Fragmented Spin Ice and Multi- k Ordering in Rare-Earth Antiperovskites

Attila Szabó^{1,2}, Fabio Orlandi², and Pascal Manuel²

¹*Rudolf Peierls Centre for Theoretical Physics, University of Oxford, Oxford OX1 3PU, United Kingdom*

²*ISIS Facility, Rutherford Appleton Laboratory, Harwell Campus, Didcot OX11 0QX, United Kingdom*

(Received 2 May 2022; accepted 31 October 2022; published 8 December 2022)

We study near-neighbor and dipolar Ising models on a lattice of corner-sharing octahedra. In an extended parameter range of both models, frustration between antiferromagnetism and a spin-ice-like three-in-three-out rule stabilizes a Coulomb phase with correlated dipolar and quadrupolar spin textures, both yielding distinctive neutron-scattering signatures. Strong further-neighbor perturbations cause the two components to order independently, resulting in unusual multi- k orders. We propose experimental realizations of our model in rare-earth antiperovskites.

DOI: 10.1103/PhysRevLett.129.247201

Spin ice has been a paradigmatic example of frustrated magnetism since its experimental realization in the rare-earth pyrochlores $\text{Dy}_2\text{Ti}_2\text{O}_7$ and $\text{Ho}_2\text{Ti}_2\text{O}_7$ [1–3]. It is defined on a lattice of corner-sharing tetrahedra by a local two-in-two-out (2I2O) constraint on each tetrahedron. This constraint results in extensive ground-state degeneracy [2,4–6], long-range dipolar correlations [7–9], and fractionalized excitations that behave as emergent magnetic monopoles [10–15], a phenomenology known as the Coulomb phase [16,17]. Spin ice, and derivatives such as quantum spin ice [10,18,19] and monopole-crystalline fragmented spin ice [20–22], are among the best-studied frustrated magnets due to the abundance of rare-earth pyrochlore materials with large local moments [23].

Nevertheless, Coulomb phases are not limited to the pyrochlore lattice, as shown by the rich physics of (artificial) square ice [24] and kagome ice [25] in two dimensions. A three-dimensional alternative would be a lattice of corner-sharing octahedra (e.g., the edge midpoints of a simple cubic lattice), endowed with Ising spins pointing into or out of these octahedra and a local three-in-three-out (3I3O) constraint, defining a 20-vertex model [26]; understanding this rule as a local divergence-free constraint yields a Coulomb phase similar to pyrochlore ice. This geometry is realized in the cubic phase of antiperovskites in which rare-earth metal ions with strong easy-axis anisotropy form coordination octahedra around a central anion [Fig. 1(a)]. Such models have received some theoretical attention [10,27,28] but have not yet been considered as an experimentally viable platform for spin ice, as realizing the perfect Coulomb phase requires significant fine-tuning.

Our Letter addresses this gap by studying both near-neighbor exchange and dipolar Ising Hamiltonians on the antiperovskite lattice. For the former, we find an extended parameter range in which frustration between antiferromagnetic alignment and the 3I3O rule brings about a new

kind of Coulomb phase. Octahedra in its ground-state manifold show correlated dipolar and quadrupolar alignment, both of which give rise to distinctive features in the magnetic structure factor. This phase, dubbed fragmented

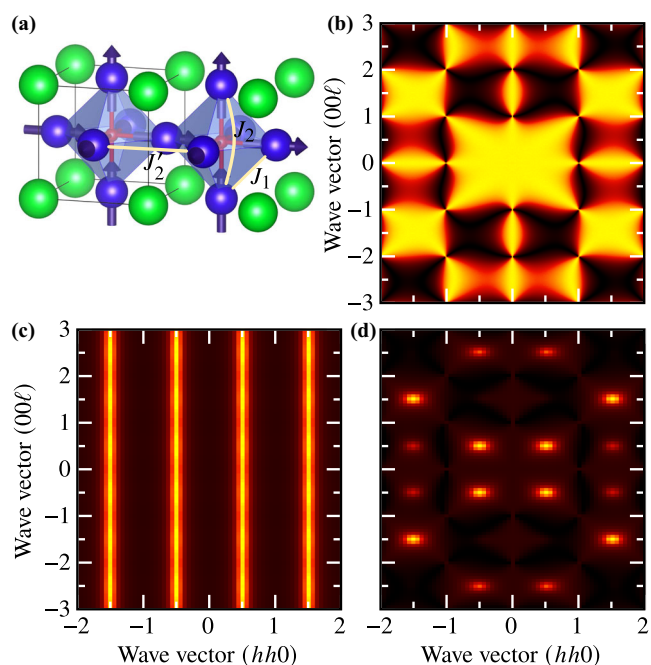


FIG. 1. (a) Two unit cells of the antiperovskite structure showing the local $\langle 100 \rangle$ Ising axes and near-neighbor exchange couplings J_1 , J_2 , J_2' of the magnetic ions (blue). (b) Spin-flip (SF) neutron-scattering pattern of (1) at $T \ll J$ for neutrons polarized along $[1\bar{1}0]$. Sharp pinch points are visible at all Γ points of the simple cubic lattice. [The non-spin-flip (NSF) structure factor is independent of wave vector.] (c) NSF and (d) SF neutron-scattering pattern of (2) for $J_2 < J_1$ at $T \rightarrow 0$. In addition to pinch points, rods of diffuse scattering arise along wave vectors of the form $(1/2, 1/2, \ell)$, which are fully visible in the NSF pattern and yield smooth maxima in the SF one.

spin ice, is further stabilized by dipolar interactions against weak further-neighbor interactions. Stronger perturbations result in a variety of ordered phases: in those derived from fragmented ice, the dipolar and quadrupolar components order independently, resulting in unusual multi- k structures.

Our results mark out rare-earth antiperovskites, with large Ising-like moments, as well as structural analogs [29,30], as a novel platform for realizing Coulomb-phase physics and may explain experiments that found no magnetic ordering in such materials down to the lowest temperatures [31,32]. Moreover, they demonstrate that the mechanisms underlying dipolar pyrochlore spin ice [6,33,34] are generic and may help stabilize more exotic icelike models [27,35–37] in the theoretical literature.

Near-neighbor exchange model.—We consider Ising spins on the X sites of a cubic perovskite (ABX_3) lattice, which form corner-sharing octahedra. The only crystallographically allowed Ising axis connects the octahedron centers, i.e., each spin points out of one octahedron into the other. The closest analog of nearest-neighbor spin ice in this geometry is a 20-vertex Ising model in which all 3I3O octahedra have equal and minimal energy,

$$H = \frac{J}{2} \sum_{\text{octah.} o} \left(\sum_{i \in o} \vec{\sigma}_i \cdot \hat{e}_{\text{out}} \right)^2, \quad (1)$$

where \hat{e}_{out} is the unit vector pointing out of octahedron o at site i and $\vec{\sigma}_i$ is constrained to be $\pm \hat{e}_{\text{out}}$. Since nearest-neighbor Ising spins are perpendicular, Heisenberg interactions between them would be inactive. Therefore, realizing (1) requires either Dzyaloshinskii-Moriya (DM) or symmetric off-diagonal exchange of equal strength to the ferromagnetic cross-octahedron interaction [$J = J_1 = J_2$, cf. Fig. 1(a)],

$$H = J_1 \sum_{\langle ij \rangle} \hat{d}_{ij} \cdot (\vec{\sigma}_i \times \vec{\sigma}_j) - J_2 \sum_{\langle\langle i \leftrightarrow j \rangle\rangle} \vec{\sigma}_i \cdot \vec{\sigma}_j + \text{const}; \quad (2)$$

the DM vector $\hat{d}_{ij} = \hat{e}_{\text{out},i} \times \hat{e}_{\text{out},j}$ is the only one allowed by lattice symmetry [38].

We computed thermodynamic properties of Eq. (1) on a system of 64^3 unit cells using an efficient cluster Monte Carlo algorithm adapted from Ref. [39] and plotted heat capacity and entropy as a function of temperature in Fig. 2. The heat capacity shows a single Schottky peak at $T \sim J$, corresponding to the proliferation of non-3I3O octahedra, viz. emergent monopoles. This Schottky peak does not account for the full high-temperature entropy of the system; the numerically obtained residual entropy is in good agreement with the Pauling estimate [4] for the 20-vertex model, $S_0 = k_B \log(2.5)/3 \approx 0.305k_B$ per spin.

Similar to pyrochlore ice, long-wavelength properties of this ground-state manifold can be understood by coarse-graining the spins $\vec{\sigma}$ into a polarization field \vec{P} . The free

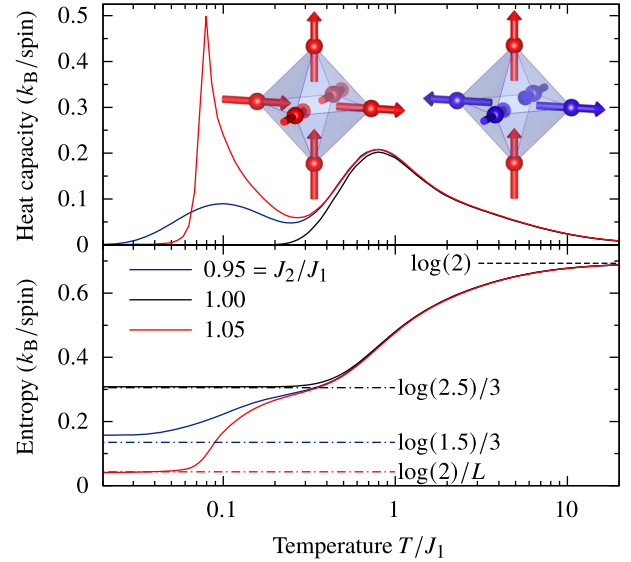


FIG. 2. Heat capacity (top) and entropy (bottom) of (2) for three values of J_2/J_1 . Inset: a ferromagnetic (left) and a dipolar-quadrupolar (right) octahedron; red spins are in dipolar, blue in quadrupolar alignment.

energy density of this field is purely entropic in origin and, in the first approximation, proportional to $|\vec{P}|^2$. Together with the divergence-free constraint $\nabla \cdot \vec{P} = 0$ imposed by the 3I3O rule, this gives rise to long-range dipolar correlations [8,9,16], which can be observed as sharp pinch points in the magnetic structure factor at reciprocal lattice vectors [Fig. 1(b)]. Non-3I3O defects are sources of the \vec{P} field and, in dipolar systems, act as emergent monopoles of the physical magnetic field [11].

The above Coulomb-phase description, however, only holds for the fine-tuned point (1). For $J_2 > J_1$, ferromagnetic alignment between spins across an octahedron is favored. Such alignment is compatible with the 3I3O rule: namely, one spin points in and one out along each body diagonal of the octahedron (see inset of Fig. 2). This alignment across each octahedron results in ground states with ferromagnetically aligned chains along all $\langle 100 \rangle$ directions. These chains are, however, decoupled, leading to uniform planes of diffuse neutron scattering at $\{hkL\}$ ($L \in \mathbb{Z}$)-type wave vectors [30,40] and a subextensive ground-state entropy of $k_B \log 2 \times 3L^2$ per L^3 unit cells: this entropy is indeed found in loop-update [34] Monte Carlo simulations of (2) with $L = 16$ (Fig. 2). The heat capacity peak at $T \sim (J_2 - J_1)$ suggests that the chains align in a Kasteleyn transition resembling that of pyrochlore spin ice in a $[100]$ field [41].

$J_2 < J_1$, by contrast, favors 3I3O octahedra that are antiferromagnetic as possible. However, if all three pairs of opposite spins are antiferromagnetically aligned (i.e., both point in or both out), the total number of spins pointing into the octahedron is even, which frustrates the 3I3O rule. For

$0 < J_2 < J_1$, the optimal octahedra are still 3I3O, but not fully antiferromagnetic, pairs across the octahedron being two-in, two-out, and one-in-one-out. There are 12 such “dipolar-quadrupolar” octahedra, so the ground-state entropy remains extensive: Pauling’s estimate yields $S'_0 = k_B \log(1.5)/3 \approx 0.135k_B$ per spin, which is in good agreement with Monte Carlo simulations (Fig. 2). Entropy is released in two Schottky peaks: at $T \sim J_{1,2}$, the high-temperature paramagnet crosses over into 20-vertex spin ice, while at $T \sim (J_1 - J_2)$, the 12-vertex ground-state manifold is selected out of the latter. Dipolar components in this manifold still form a Coulomb phase: pinch points remain sharp but their intensity is reduced due to the smaller average dipole moment of dipolar-quadrupolar octahedra [Fig. 1(d)]. The antiferromagnetic quadrupolar components, on the other hand, enhance the magnetic structure factor in rods at $(1/2, 1/2, \ell)$ and similar wave vectors without new singular features. Such fragmentation *within* the ice manifold has no analog on the pyrochlore lattice, and, as quadrupoles do not contribute to the coarse-grained field \vec{P} , it is not fully captured by Coulomb-phase theory.

Dipolar spin ice.—Next, we consider adding dipolar interactions between the large rare-earth Ising moments,

$$H = D\ell^3 \sum_{ij} \left[\frac{\vec{\sigma}_i \cdot \vec{\sigma}_j}{r_{ij}^3} - \frac{3(\vec{\sigma}_i \cdot \vec{r}_{ij})(\vec{\sigma}_j \cdot \vec{r}_{ij})}{r_{ij}^5} \right] - J_2 \sum_{\langle\langle i \leftrightarrow j \rangle\rangle} \vec{\sigma}_i \cdot \vec{\sigma}_j - J'_2 \sum_{\langle\langle ij \rangle\rangle} \vec{\sigma}_i \cdot \vec{\sigma}_j, \quad (3)$$

where ℓ is the distance of nearest-neighbor spins and $D = \mu_0 \mu^2 / (4\pi \ell^3)$ is the dipolar interaction-energy scale. For simplicity, we set $J_1 = 0$; indeed, adding multiples of (1) to the Hamiltonian only renormalizes the energy cost of monopoles, so low-temperature effects of J_1 and J_2 are equivalent. On the other hand, we add second-neighbor interactions between spins in different octahedra [J'_2 in Fig. 1(a)] as a representative of all subleading exchange couplings; in antiperovskite materials, we expect $J'_2 \ll J_2$ as there is no obvious exchange pathway between 2' neighbors.

On the pyrochlore lattice, dipolar interactions can be decomposed into a leading term that leaves the monopole-free sector exactly degenerate and residual interactions that decay as r^{-5} and are thus negligible beyond nearest neighbors [33]: that is, the two-in-two-out manifold in dipolar pyrochlore ice remains degenerate to a good approximation. A similar decomposition of the dipolar Hamiltonian is possible on the antiperovskite lattice as well [42]; however, as the nearest-neighbor residual interaction is much stronger than that across an octahedron, a purely dipolar Hamiltonian would be projectively equivalent to the 12-vertex model found above for $J_2 < J_1$ [42]. Emulating the 20-vertex Coulomb phase requires compensating the

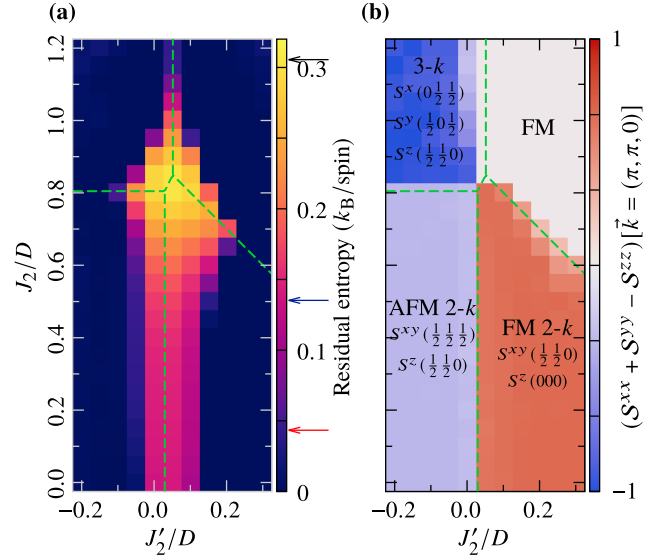


FIG. 3. (a) Residual entropy at $T = 0.25D$ (below spin freezing) in single-spin-flip dynamics. The colored arrows indicate the Pauling entropy estimates of the near-neighbor model (2). (b) Composite order parameter of the four ordered phases at $T = 0.1D$ in loop-update dynamics, which remains in equilibrium down to this temperature. AFM, antiferromagnetic; FM, ferromagnetic.

residual terms with a ferromagnetic $J'_2 \approx 0.75D$ [42]; indeed, the entire 3I3O manifold is approximately degenerate at this point, evidenced by the confluence of all ordered phases in Fig. 3(b).

Using single-spin-flip Monte Carlo dynamics [6], we indeed find an extensive residual entropy for $J_2 \lesssim J_2^*$, $J'_2 \approx 0$. At $J_2 \approx J_2^*$, the residual entropy is consistent with that of the 20-vertex model; as J_2 is lowered, this value decreases continuously to the residual entropy of the 12-vertex fragmented spin ice of dipolar-quadrupolar octahedra [Fig. 3(a)]. These icelike phases are stabilized by the dipolar interactions, which cause the single-spin-flip dynamics (realized in materials by thermal fluctuations) to become glassy [42], thus preventing any low-temperature ordering transition, similar to dipolar pyrochlore ice [34,50–54]. Indeed, simulations using loop-update dynamics find ordered ground states with zero residual entropy for all values of J_2 and J'_2 [Fig. 3(b)].

Magnetic structure factors in the high-residual-entropy regime resemble closely those of the J_1 - J_2 model above. Neutron-scattering patterns at $J_2 \approx J_2^*$ are similar to those of (1) [42], while the $J_2 < J_2^*$ case (Fig. 4) resembles the 12-vertex model [Figs. 1(c) and 1(d)], with two important differences. First, dipolar pinch points have higher intensity, while the broad quadrupolar maxima at $(1/2, 1/2, 1/2)$ are weaker. Second, sharp peaks appear at $(1/2, 1/2, 0)$ due to ordering of the quadrupolar components of the octahedra; however, the ordered moment remains quite small, as evidenced by a substantial diffuse component

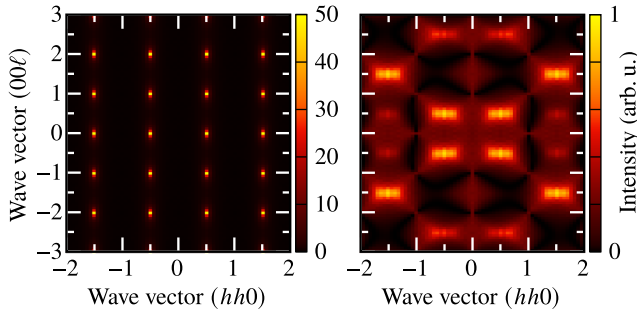


FIG. 4. Polarized neutron-scattering pattern of (3) at $J_2 = 0.4D$, $J'_2 = 0.05D$. Neutrons are polarized along $[1\bar{1}0]$. The non-spin-flip channel (left) is strongly peaked at $(1/2, 1/2, 0)$, with some visible broadening along the q_z direction. The spin-flip channel (right) remains diffuse, with pinch points at Γ and smooth intensity maxima at $(1/2, 1/2, 1/2)$.

surrounding the peaks. Both effects are due to the low-temperature glassiness of single-spin-flip dynamics, which sabotages both the full suppression of ferromagnetic octahedra and the full development of order.

Ordered phases.—Such spin freezing can effectively be lifted in Monte Carlo simulations by adding short-loop updates that respect the 3I3O ice rules [34]. These reveal four low-temperature ordered phases that all meet near the optimally compensated spin-ice point [Fig. 3(b)]. At $J_2 \gtrsim J_2^*$, ferromagnetic octahedra are favorable, resulting in aligned chains of spins, similar to the proposed ground states of pyrochlore ice [34,55,56]. If $J'_2 \gtrsim 0$, these chains

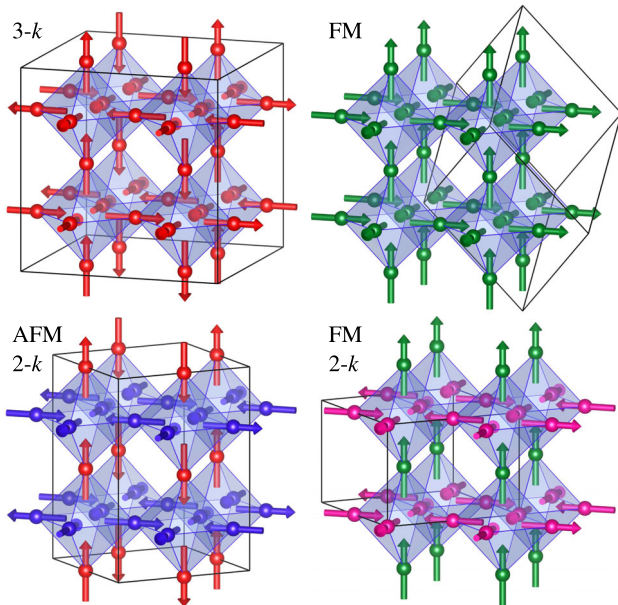


FIG. 5. Magnetic structures of the four ordered phases in Fig. 3(b). Colors indicate inequivalent ordering wave vectors: green, (000); blue, $(1/2, 1/2, 1/2)$; red, $(1/2, 1/2, 0)$ normal to spin direction; purple, $(1/2, 1/2, 0)$ in the plane of spin directions. The black boxes indicate the magnetic unit cell of each order.

align into a three-dimensional canted ferromagnet; for antiferromagnetic J'_2 , each sublattice orders along the $\{1/2, 1/2, 0\}$ wave vector normal to its spin direction, resulting in a three- k structure with full cubic symmetry. Both transitions are strongly first-order [42], similar to dipolar pyrochlore ice [34].

On the other hand, phases at $J_2 \lesssim J_2^*$ are composed of dipolar-quadrupolar octahedra: the two components order independently, which breaks cubic rotational symmetry and results in two- k structures. Ordering wave vectors are again controlled by the sign of J'_2 , as shown in Fig. 5; neutron-scattering signatures of the ordered phases are discussed in the Supplemental Material [42]. As the ordered state is described by two independent order parameters with distinct symmetries, the ordering transition occurs in two stages: first, quadrupolar components order in a continuous transition, followed by the dipolar ones at a lower temperature, which leads to a jump in both order parameters [42]. Between these transitions, we anticipate another kind of fragmented spin ice, in which the quadrupolar components show partial ordering, while dipolar ones remain in a Coulomb phase.

Conclusion.—In summary, we have studied dipolar and purely near-neighbor exchange Ising models on a lattice of corner-sharing octahedra, as may be realized in rare-earth antiperovskite materials. Similar to spin ice on the pyrochlore lattice, the phase diagram of these systems can be understood in terms of a 20-vertex model of three-in-three-out octahedra, which gives rise to a low-temperature Coulomb phase with extensive ground-state entropy, pinch-point correlations, and emergent magnetic monopoles. While such a model is fine-tuned, glassiness induced by dipolar interactions in spin ice stabilizes the Coulomb phase for a finite range of exchange parameters. More interestingly, perturbing away from this fine-tuned point results in fragmented spin ice, where spins around each octahedron exhibit both dipolar and quadrupolar alignment; while the former remain in a Coulomb phase, the latter also contribute distinctive features to structure factors. Such a fragmented phase is not possible in pyrochlore ice (except in strained thin films [57,58]), as all 2I2O tetrahedra are symmetry-equivalent to one another; by contrast, it is generic on the antiperovskite lattice as it is stabilized by the dipolar interaction for a wide and experimentally relevant range of parameters. Further-neighbor interactions break the approximate degeneracy of these ice manifolds, resulting in a variety of ordered phases. In particular, perturbing the fragmented spin ice gives rise to two- k structures as the dipolar and quadrupolar components yield symmetry-inequivalent order parameters at different propagation vectors and thus two distinct ordering transitions at different temperatures.

Our results demonstrate that both mechanisms by which dipolar interactions stabilize pyrochlore ice, the projective equivalence of dipolar and near-neighbor exchange models

[6,33] and glassy low-temperature spin dynamics [34,50,51], remain active on other lattices and help stabilize analogous Coulomb phases. This is critical for antiperovskite materials, as the projective-equivalence mechanism is insensitive to low-temperature distortions of the crystal structure [59] and may also help stabilize more complex models, several of which exhibit fractonic features [27,37].

In fact, lattices beyond the pyrochlore may exhibit richer physics, precisely on account of the several interaction terms that need to be fine-tuned to realize the perfect Coulomb phase. A case in point is the antiperovskite lattice, where frustration between antiferromagnetic correlations and the 3I3O rule results in fragmented spin ice, without direct analogs in bulk pyrochlores. This opens up new experimental directions for frustrated magnetism: indeed, certain rare-earth antiperovskites are known to avoid magnetic ordering down to very low temperatures [31,32], which may indicate spin-ice physics. On the theoretical side, developing field theories for the fragmented ice phase promises considerable challenges due to the frustration needed to bring it about. (The long-wavelength physics of Coulomb phases is essentially unfrustrated [8,9].) The coexistence of dipolar and quadrupolar features also raises the possibility of a higher-order gauge theory description, with potentially exciting consequences for both excitations and ordering transitions.

All data supporting this work and the code used to generate them are available on Zenodo [60,61].

We thank Claudio Castelnovo, Dmitry Khalyavin, and Étienne Lantagne-Hurtubise for useful discussions. Figures 1(a) and 5 were made using VESTA [62]. All heat maps use perceptually uniform color maps developed in Ref. [63]. A. S. gratefully acknowledges the ISIS Neutron and Muon Source and the Oxford–ShanghaiTech Collaboration for support of the Keeley-Rutherford fellowship at Wadham College, Oxford. Computing resources were provided by STFC Scientific Computing Department’s SCARF cluster.

[1] M. J. Harris, S. T. Bramwell, D. F. McMorrow, T. Zeiske, and K. W. Godfrey, Geometrical Frustration in the Ferromagnetic Pyrochlore Ho₂Ti₂O₇, *Phys. Rev. Lett.* **79**, 2554 (1997).
 [2] A. P. Ramirez, A. Hayashi, R. J. Cava, R. Siddharthan, and B. S. Shastry, Zero-point entropy in ‘spin ice’, *Nature (London)* **399**, 333 (1999).
 [3] S. T. Bramwell and M. J. Gingras, Spin ice state in frustrated magnetic pyrochlore materials, *Science* **294**, 1495 (2001).
 [4] L. Pauling, The structure and entropy of ice and of other crystals with some randomness of atomic arrangement, *J. Am. Chem. Soc.* **57**, 2680 (1935).
 [5] P. W. Anderson, Ordering and antiferromagnetism in ferrites, *Phys. Rev.* **102**, 1008 (1956).

[6] B. C. den Hertog and M. J. P. Gingras, Dipolar Interactions and Origin of Spin Ice in Ising Pyrochlore Magnets, *Phys. Rev. Lett.* **84**, 3430 (2000).
 [7] S. T. Bramwell, M. J. Harris, B. C. den Hertog, M. J. P. Gingras, J. S. Gardner, D. F. McMorrow, A. R. Wildes, A. L. Cornelius, J. D. M. Champion, R. G. Melko, and T. Fennell, Spin Correlations in Ho₂Ti₂O₇: A Dipolar Spin Ice System, *Phys. Rev. Lett.* **87**, 047205 (2001).
 [8] S. V. Isakov, K. Gregor, R. Moessner, and S. L. Sondhi, Dipolar Spin Correlations in Classical Pyrochlore Magnets, *Phys. Rev. Lett.* **93**, 167204 (2004).
 [9] C. L. Henley, Power-law spin correlations in pyrochlore antiferromagnets, *Phys. Rev. B* **71**, 014424 (2005).
 [10] M. Hermele, M. P. A. Fisher, and L. Balents, Pyrochlore photons: The U(1) spin liquid in a $S = 1/2$ three-dimensional frustrated magnet, *Phys. Rev. B* **69**, 064404 (2004).
 [11] C. Castelnovo, R. Moessner, and S. L. Sondhi, Magnetic monopoles in spin ice, *Nature (London)* **451**, 42 (2008).
 [12] D. J. P. Morris, D. A. Tennant, S. A. Grigera, B. Klemke, C. Castelnovo, R. Moessner, C. Czternasty, M. Meissner, K. C. Rule, J.-U. Hoffmann, K. Kiefer, S. Gerischer, D. Slobinsky, and R. S. Perry, Dirac strings and magnetic monopoles in the spin ice Dy₂Ti₂O₇, *Science* **326**, 411 (2009).
 [13] T. Fennell, P. P. Deen, A. R. Wildes, K. Schmalzl, D. Prabhakaran, A. T. Boothroyd, R. J. Aldus, D. F. McMorrow, and S. T. Bramwell, Magnetic Coulomb phase in the Spin Ice Ho₂Ti₂O₇, *Science* **326**, 415 (2009).
 [14] S. T. Bramwell, S. R. Giblin, S. Calder, R. J. Aldus, D. Prabhakaran, and T. Fennell, Measurement of the charge and current of magnetic monopoles in spin ice, *Nature (London)* **461**, 956 (2009).
 [15] R. Dusad, F. K. K. Kirschner, J. C. Hoke, B. R. Roberts, A. Eyal, F. Flicker, G. M. Luke, S. J. Blundell, and J. C. S. Davis, Magnetic monopole noise, *Nature (London)* **571**, 234 (2019).
 [16] C. L. Henley, The “Coulomb phase” in frustrated systems, *Annu. Rev. Condens. Matter Phys.* **1**, 179 (2010).
 [17] C. Castelnovo, R. Moessner, and S. L. Sondhi, Spin ice, fractionalization, and topological order, *Annu. Rev. Condens. Matter Phys.* **3**, 35 (2012).
 [18] M. J. Gingras and P. A. McClarty, Quantum spin ice: A search for gapless quantum spin liquids in pyrochlore magnets, *Rep. Prog. Phys.* **77**, 056501 (2014).
 [19] J. G. Rau and M. J. Gingras, Frustrated quantum rare-earth pyrochlores, *Annu. Rev. Condens. Matter Phys.* **10**, 357 (2019).
 [20] E. Lefrançois, V. Cathelin, E. Lhotel, J. Robert, P. Lejay, C. V. Colin, B. Canals, F. Damay, J. Ollivier, B. Fåk, L. C. Chapon, R. Ballou, and V. Simonet, Fragmentation in spin ice from magnetic charge injection, *Nat. Commun.* **8**, 209 (2017).
 [21] V. Cathelin, E. Lefrançois, J. Robert, P. C. Guruciaga, C. Paulsen, D. Prabhakaran, P. Lejay, F. Damay, J. Ollivier, B. Fåk, L. C. Chapon, R. Ballou, V. Simonet, P. C. W. Holdsworth, and E. Lhotel, Fragmented monopole crystal, dimer entropy and Coulomb interactions in Dy₂Ir₂O₇, *Phys. Rev. Res.* **2**, 032073(R) (2020).
 [22] M. J. Pearce, K. Götze, A. Szabó, T. S. Sikkenk, M. R. Lees, A. T. Boothroyd, D. Prabhakaran, C. Castelnovo, and

- P. A. Goddard, Monopole density and antiferromagnetic domain control in spin-ice iridates, *Nat. Commun.* **13**, 444 (2022).
- [23] C. R. Wiebe and A. M. Hallas, Frustration under pressure: Exotic magnetism in new pyrochlore oxides, *APL Mater.* **3**, 041519 (2015).
- [24] C. Nisoli, R. Moessner, and P. Schiffer, Colloquium: Artificial spin ice: Designing and imaging magnetic frustration, *Rev. Mod. Phys.* **85**, 1473 (2013).
- [25] K. Zhao, H. Deng, H. Chen, K. A. Ross, V. Petricek, G. Günther, M. Russina, V. Hutanu, and P. Gegenwart, Realization of the kagome spin ice state in a frustrated intermetallic compound, *Science* **367**, 1218 (2020).
- [26] R. J. Baxter, *Exactly Solved Models in Statistical Mechanics* (Academic Press, London, 1982).
- [27] O. Benton and R. Moessner, Topological Route to New and Unusual Coulomb Spin Liquids, *Phys. Rev. Lett.* **127**, 107202 (2021).
- [28] S. R. Sklan and C. L. Henley, Nonplanar ground states of frustrated antiferromagnets on an octahedral lattice, *Phys. Rev. B* **88**, 024407 (2013).
- [29] C. S. Coates, M. Baise, A. Schmutzler, A. Simonov, J. W. Makepeace, A. G. Seel, R. I. Smith, H. Y. Playford, D. A. Keen, R. Siegel, J. Senker, B. Slater, and A. L. Goodwin, Spin-ice physics in cadmium cyanide, *Nat. Commun.* **12**, 2272 (2021).
- [30] A. R. Overy, A. B. Cairns, M. J. Cliffe, A. Simonov, M. G. Tucker, and A. L. Goodwin, Design of crystal-like aperiodic solids with selective disorder–phonon coupling, *Nat. Commun.* **7**, 10445 (2016).
- [31] H. A. Höpfe, G. Kotzyba, R. Pöttgen, and W. Schnick, Synthesis, crystal structure, magnetism, and optical properties of Gd₃[SiON₃]O—an oxonitridosilicate oxide with non-condensed SiON₃ tetrahedra, *J. Solid State Chem.* **167**, 393 (2002).
- [32] S. D. Kloth, N. Weidmann, and W. Schnick, Antiperovskite nitridophosphate oxide Ho₃[PN₄]O by high-pressure meta-thesis, *Eur. J. Inorg. Chem.* **2017**, 1930 (2017).
- [33] S. V. Isakov, R. Moessner, and S. L. Sondhi, Why Spin Ice Obeys the Ice Rules, *Phys. Rev. Lett.* **95**, 217201 (2005).
- [34] R. G. Melko and M. J. Gingras, Monte Carlo studies of the dipolar spin ice model, *J. Phys. Condens. Matter* **16**, R1277 (2004).
- [35] E. Lantagne-Hurtubise, J. G. Rau, and M. J. P. Gingras, Spin-Ice Thin Films: Large-*n* Theory and Monte Carlo Simulations, *Phys. Rev. X* **8**, 021053 (2018).
- [36] H. Yan, O. Benton, L. D. C. Jaubert, and N. Shannon, Rank-2 *u*(1) Spin Liquid on the Breathing Pyrochlore Lattice, *Phys. Rev. Lett.* **124**, 127203 (2020).
- [37] É. Lantagne-Hurtubise, H. Yan, and J. Rau (to be published).
- [38] T. Moriya, Anisotropic superexchange interaction and weak ferromagnetism, *Phys. Rev.* **120**, 91 (1960).
- [39] H. Otsuka, Cluster algorithm for Monte Carlo simulations of spin ice, *Phys. Rev. B* **90**, 220406(R) (2014).
- [40] R. Comès, M. Lambert, and A. Guinier, Désordre linéaire dans les cristaux (cas du silicium, du quartz, et des pérovskites ferroélectriques), *Acta Cryst. A* **26**, 244 (1970).
- [41] L. D. C. Jaubert, J. T. Chalker, P. C. W. Holdsworth, and R. Moessner, Three-Dimensional Kasteleyn Transition: Spin Ice in a [100] Field, *Phys. Rev. Lett.* **100**, 067207 (2008).
- [42] See Supplemental Material at <http://link.aps.org/supplemental/10.1103/PhysRevLett.129.247201> for details of the Monte Carlo simulations, autocorrelation times, the projective-equivalence mechanism, the thermodynamics of dipolar spin ice, the ordered phases (including mcif files) and ordering transitions, and additional neutron-scattering patterns. The Supplementary Material includes additional Refs. [43–49].
- [43] S. W. de Leeuw, J. W. Perram, and E. R. Smith, Simulation of electrostatic systems in periodic boundary conditions. I. Lattice sums and dielectric constants, *Proc. R. Soc. A* **373**, 27 (1980).
- [44] H. Otsuka, Loop-string algorithm for Monte Carlo simulations of dipolar spin ice, *Phys. Rev. B* **92**, 134401 (2015).
- [45] K. T. K. Chung, J. S. K. Goh, A. Mukherjee, W. Jin, D. Lozano-Gómez, and M. J. P. Gingras, Probing Flat Band Physics in Spin Ice Systems via Polarized Neutron Scattering, *Phys. Rev. Lett.* **128**, 107201 (2022).
- [46] W. Opechowski and R. Guccione, *Magnetism*, edited by G. T. Rado and H. Suhl (Academic Press, New York, 1965), Vol. IIA.
- [47] S. C. Miller and W. F. Love, *Tables of Irreducible Representations of Space Groups and Co-Representations of Magnetic Space Groups* (Pruett, Boulder, 1967).
- [48] B. J. Campbell, H. T. Stokes, D. E. Tanner, and D. M. Hatch, ISODISPLACE: A web-based tool for exploring structural distortions, *J. Appl. Crystallogr.* **39**, 607 (2006).
- [49] D. M. Hatch and H. T. Stokes, INVARIANTS: Program for obtaining a list of invariant polynomials of the order-parameter components associated with irreducible representations of a space group, *J. Appl. Crystallogr.* **36**, 951 (2003).
- [50] J. Snyder, B. G. Ueland, J. S. Slusky, H. Karunadasa, R. J. Cava, and P. Schiffer, Low-temperature spin freezing in the Dy₂Ti₂O₇ spin ice, *Phys. Rev. B* **69**, 064414 (2004).
- [51] L. D. C. Jaubert and P. C. W. Holdsworth, Signature of magnetic monopole and Dirac string dynamics in spin ice, *Nat. Phys.* **5**, 258 (2009).
- [52] L. D. C. Jaubert and P. C. W. Holdsworth, Magnetic monopole dynamics in spin ice, *J. Phys. Condens. Matter* **23**, 164222 (2011).
- [53] B. Tomasello, C. Castelnovo, R. Moessner, and J. Quintanilla, Correlated Quantum Tunneling of Monopoles in Spin Ice, *Phys. Rev. Lett.* **123**, 067204 (2019).
- [54] J. N. Hallén, S. A. Grigera, D. A. Tennant, C. Castelnovo, and R. Moessner, Dynamical fractal and anomalous noise in a clean magnetic crystal, [arXiv:2211.00051](https://arxiv.org/abs/2211.00051).
- [55] P. A. McClarty, O. Sikora, R. Moessner, K. Penc, F. Pollmann, and N. Shannon, Chain-based order and quantum spin liquids in dipolar spin ice, *Phys. Rev. B* **92**, 094418 (2015).
- [56] P. Henelius, T. Lin, M. Enjalran, Z. Hao, J. G. Rau, J. Altosaar, F. Flicker, T. Yavors'kii, and M. J. P. Gingras, Refrustration and competing orders in the prototypical

- Dy₂Ti₂O₇ spin ice material, *Phys. Rev. B* **93**, 024402 (2016).
- [57] L. D. C. Jaubert, T. Lin, T. S. Opel, P. C. W. Holdsworth, and M. J. P. Gingras, Spin Ice Thin Film: Surface Ordering, Emergent Square Ice, and Strain Effects, *Phys. Rev. Lett.* **118**, 207206 (2017).
- [58] L. Bovo, C. M. Rouleau, D. Prabhakaran, and S. T. Bramwell, Phase transitions in few-monolayer spin ice films, *Nat. Commun.* **10**, 1219 (2019).
- [59] A. M. Glazer, The classification of tilted octahedra in perovskites, *Acta Crystallogr. Sect. B* **28**, 3384 (1972).
- [60] A. Szabó, F. Orlandi, and P. Manuel, Monte Carlo simulations of octahedral spin ice (2022), [10.5281/zenodo.7293218](https://doi.org/10.5281/zenodo.7293218).
- [61] A. Szabó, Monte Carlo simulation library for octahedral spin ice (2022), [10.5281/zenodo.7295313](https://doi.org/10.5281/zenodo.7295313).
- [62] K. Momma and F. Izumi, VESTA 3 for three-dimensional visualization of crystal, volumetric and morphology data, *J. Appl. Crystallogr.* **44**, 1272 (2011).
- [63] P. Kovesi, Good colour maps: How to design them, [arXiv:1509.03700](https://arxiv.org/abs/1509.03700).